

# Search for Invisible Decays of $\eta$ and $\eta'$ in the Processes $J/\psi \rightarrow \phi\eta$ and $\phi\eta'$

M. Ablikim<sup>1</sup>, J. Z. Bai<sup>1</sup>, Y. Ban<sup>12</sup>, J. G. Bian<sup>1</sup>, X. Cai<sup>1</sup>, H. F. Chen<sup>17</sup>, H. S. Chen<sup>1</sup>, H. X. Chen<sup>1</sup>, J. C. Chen<sup>1</sup>, Jin Chen<sup>1</sup>, Y. B. Chen<sup>1</sup>, S. P. Chi<sup>2</sup>, Y. P. Chu<sup>1</sup>, X. Z. Cui<sup>1</sup>, Y. S. Dai<sup>19</sup>, L. Y. Diao<sup>9</sup>, Z. Y. Deng<sup>1</sup>, Q. F. Dong<sup>15</sup>, S. X. Du<sup>1</sup>, J. Fang<sup>1</sup>, S. S. Fang<sup>2</sup>, C. D. Fu<sup>1</sup>, C. S. Gao<sup>1</sup>, Y. N. Gao<sup>15</sup>, S. D. Gu<sup>1</sup>, Y. T. Gu<sup>4</sup>, Y. N. Guo<sup>1</sup>, Y. Q. Guo<sup>1</sup>, Z. J. Guo<sup>16</sup>, F. A. Harris<sup>16</sup>, K. L. He<sup>1</sup>, M. He<sup>13</sup>, Y. K. Heng<sup>1</sup>, H. M. Hu<sup>1</sup>, T. Hu<sup>1</sup>, G. S. Huang<sup>1a</sup>, X. T. Huang<sup>13</sup>, X. B. Ji<sup>1</sup>, X. S. Jiang<sup>1</sup>, X. Y. Jiang<sup>5</sup>, J. B. Jiao<sup>13</sup>, D. P. Jin<sup>1</sup>, S. Jin<sup>1</sup>, Yi Jin<sup>8</sup>, Y. F. Lai<sup>1</sup>, G. Li<sup>2</sup>, H. B. Li<sup>1</sup>, H. H. Li<sup>1</sup>, J. Li<sup>1</sup>, R. Y. Li<sup>1</sup>, S. M. Li<sup>1</sup>, W. D. Li<sup>1</sup>, W. G. Li<sup>1</sup>, X. L. Li<sup>1</sup>, X. N. Li<sup>1</sup>, X. Q. Li<sup>11</sup>, Y. L. Li<sup>4</sup>, Y. F. Liang<sup>14</sup>, H. B. Liao<sup>1</sup>, B. J. Liu<sup>1</sup>, C. X. Liu<sup>1</sup>, F. Liu<sup>6</sup>, Fang Liu<sup>1</sup>, H. H. Liu<sup>1</sup>, H. M. Liu<sup>1</sup>, J. Liu<sup>12</sup>, J. B. Liu<sup>1</sup>, J. P. Liu<sup>18</sup>, Q. Liu<sup>1</sup>, R. G. Liu<sup>1</sup>, Z. A. Liu<sup>1</sup>, Y. C. Lou<sup>5</sup>, F. Lu<sup>1</sup>, G. R. Lu<sup>5</sup>, J. G. Lu<sup>1</sup>, C. L. Luo<sup>10</sup>, F. C. Ma<sup>9</sup>, H. L. Ma<sup>1</sup>, L. L. Ma<sup>1</sup>, Q. M. Ma<sup>1</sup>, X. B. Ma<sup>5</sup>, Z. P. Mao<sup>1</sup>, X. H. Mo<sup>1</sup>, J. Nie<sup>1</sup>, S. L. Olsen<sup>16</sup>, H. P. Peng<sup>17d</sup>, R. G. Ping<sup>1</sup>, N. D. Qi<sup>1</sup>, H. Qin<sup>1</sup>, J. F. Qiu<sup>1</sup>, Z. Y. Ren<sup>1</sup>, G. Rong<sup>1</sup>, L. Y. Shan<sup>1</sup>, L. Shang<sup>1</sup>, C. P. Shen<sup>1</sup>, D. L. Shen<sup>1</sup>, X. Y. Shen<sup>1</sup>, H. Y. Sheng<sup>1</sup>, H. S. Sun<sup>1</sup>, J. F. Sun<sup>1</sup>, S. S. Sun<sup>1</sup>, Y. Z. Sun<sup>1</sup>, Z. J. Sun<sup>1</sup>, Z. Q. Tan<sup>4</sup>, X. Tang<sup>1</sup>, G. L. Tong<sup>1</sup>, G. S. Varner<sup>16</sup>, D. Y. Wang<sup>1</sup>, L. Wang<sup>1</sup>, L. L. Wang<sup>1</sup>, L. S. Wang<sup>1</sup>, M. Wang<sup>1</sup>, P. Wang<sup>1</sup>, P. L. Wang<sup>1</sup>, W. F. Wang<sup>1b</sup>, Y. F. Wang<sup>1</sup>, Z. Wang<sup>1</sup>, Z. Y. Wang<sup>1</sup>, Zhe Wang<sup>1</sup>, Zheng Wang<sup>2</sup>, C. L. Wei<sup>1</sup>, D. H. Wei<sup>1</sup>, N. Wu<sup>1</sup>, X. M. Xia<sup>1</sup>, X. X. Xie<sup>1</sup>, G. F. Xu<sup>1</sup>, X. P. Xu<sup>6</sup>, Y. Xu<sup>11</sup>, M. L. Yan<sup>17</sup>, H. X. Yang<sup>1</sup>, Y. X. Yang<sup>3</sup>, M. H. Ye<sup>2</sup>, Y. X. Ye<sup>17</sup>, Z. Y. Yi<sup>1</sup>, G. W. Yu<sup>1</sup>, C. Z. Yuan<sup>1</sup>, J. M. Yuan<sup>1</sup>, Y. Yuan<sup>1</sup>, S. L. Zang<sup>1</sup>, Y. Zeng<sup>7</sup>, Yu Zeng<sup>1</sup>, B. X. Zhang<sup>1</sup>, B. Y. Zhang<sup>1</sup>, C. C. Zhang<sup>1</sup>, D. H. Zhang<sup>1</sup>, H. Q. Zhang<sup>1</sup>, H. Y. Zhang<sup>1</sup>, J. W. Zhang<sup>1</sup>, J. Y. Zhang<sup>1</sup>, S. H. Zhang<sup>1</sup>, X. M. Zhang<sup>1</sup>, X. Y. Zhang<sup>13</sup>, Yiyun Zhang<sup>14</sup>, Z. P. Zhang<sup>17</sup>, D. X. Zhao<sup>1</sup>, J. W. Zhao<sup>1</sup>, M. G. Zhao<sup>1</sup>, P. P. Zhao<sup>1</sup>, W. R. Zhao<sup>1</sup>, Z. G. Zhao<sup>1c</sup>, H. Q. Zheng<sup>12</sup>, J. P. Zheng<sup>1</sup>, Z. P. Zheng<sup>1</sup>, L. Zhou<sup>1</sup>, N. F. Zhou<sup>1c</sup>, K. J. Zhu<sup>1</sup>, Q. M. Zhu<sup>1</sup>, Y. C. Zhu<sup>1</sup>, Y. S. Zhu<sup>1</sup>, Yingchun Zhu<sup>1d</sup>, Z. A. Zhu<sup>1</sup>, B. A. Zhuang<sup>1</sup>, X. A. Zhuang<sup>1</sup>, B. S. Zou<sup>1</sup>

(BES Collaboration)

<sup>1</sup> *Institute of High Energy Physics, Beijing 100049, People's Republic of China*

<sup>2</sup> *China Center for Advanced Science and Technology (CCAST), Beijing 100080, People's Republic of China*

<sup>3</sup> *Guangxi Normal University, Guilin 541004, People's Republic of China*

<sup>4</sup> *Guangxi University, Nanning 530004, People's Republic of China*

<sup>5</sup> *Henan Normal University, Xinxiang 453002, People's Republic of China*

<sup>6</sup> *Huazhong Normal University, Wuhan 430079, People's Republic of China*

<sup>7</sup> *Hunan University, Changsha 410082, People's Republic of China*

<sup>8</sup> *Jinan University, Jinan 250022, People's Republic of China*

<sup>9</sup> *Liaoning University, Shenyang 110036, People's Republic of China*

<sup>10</sup> *Nanjing Normal University, Nanjing 210097, People's Republic of China*

<sup>11</sup> *Nankai University, Tianjin 300071, People's Republic of China*

<sup>12</sup> *Peking University, Beijing 100871, People's Republic of China*

<sup>13</sup> *Shandong University, Jinan 250100, People's Republic of China*

<sup>14</sup> *Sichuan University, Chengdu 610064, People's Republic of China*

<sup>15</sup> *Tsinghua University, Beijing 100084, People's Republic of China*

<sup>16</sup> *University of Hawaii, Honolulu, HI 96822, USA*

<sup>17</sup> *University of Science and Technology of China, Hefei 230026, People's Republic of China*

<sup>18</sup> *Wuhan University, Wuhan 430072, People's Republic of China*

<sup>19</sup> *Zhejiang University, Hangzhou 310028, People's Republic of China*

<sup>a</sup> *Current address: Purdue University, West Lafayette, IN 47907, USA*

<sup>b</sup> *Current address: Laboratoire de l'Accélérateur Linéaire, Orsay, F-91898, France*

<sup>c</sup> *Current address: University of Michigan, Ann Arbor, MI 48109, USA*

<sup>d</sup> *Current address: DESY, D-22607, Hamburg, Germany*

(Dated: December 2, 2024)

We present searching for the invisible decays of  $\eta$  and  $\eta'$  in  $J/\psi$  to  $\phi\eta$  and  $\phi\eta'$ . The  $\phi$  signals are reconstructed in  $K^+K^-$  final states which are used to tag the invisible decays of  $\eta$  and  $\eta'$ . The results are obtained from data sample of  $58 \times 10^6$   $J/\psi$  decays collected with the BES II detector at the BEPC. We find no signals for the invisible decays of both  $\eta$  and  $\eta'$ . The upper limits are

established at the 90% confidence level of  $1.65 \times 10^{-3}$  for the ratio  $\frac{B(\eta \rightarrow \text{invisible})}{B(\eta \rightarrow \gamma\gamma)}$  and  $6.69 \times 10^{-2}$  for the ratio  $\frac{B(\eta' \rightarrow \text{invisible})}{B(\eta' \rightarrow \gamma\gamma)}$ . These are the first searches of the  $\eta$  and  $\eta'$  decays into invisible final states in the world.

PACS numbers: 13.25.Gv, 13.25.Jx, 14.40.Aq, 95.30.Cq

Invisible decays of quarkonium states offer a window into what may lie beyond the Standard Model. The reason is that apart from neutrinos, the minimal Standard Model predicts no other invisible final particles that these states can decay into. Many efforts on searching for invisible decays of quarkonium states had been done in order to look for the existences of possible new physics, such as extra Z-bosons, R-parity violating effects in supersymmetric Standard Model [1], and the light dark matter particle candidates [2, 3, 4, 5]. Constraint on non-interacting particles from accelerator experiments only came from CLEO, which measured the  $\Upsilon(1S) \rightarrow \gamma + \text{invisible}$  signals, giving the best sensitivity to the dark matter candidates lighter than approximately  $1.5 \text{ GeV}/c^2$  [6]. So it will be interesting to search for invisible decays of particles known to exist. While, the only particles with reported invisible branching fractions or limits are the  $\pi^0$  and Z boson [7]. We present here a simultaneous measurements of branching fractions of  $\eta$  and  $\eta'$  decays into invisible final states, or  $\nu\bar{\nu}$  within Standard Model.

The data used in this analysis were accumulated with the BES II detector [8], at the BEPC. The sample consists of  $58 \times 10^6$   $J/\psi$  decay events. BES II is a conventional solenoid magnet detector that is described in detail in Ref. [8]. A 12-layer vertex chamber (VC) surrounding the beam pipe provides trigger information. A forty-layer main drift chamber (MDC), located radially outside the VC, provides trajectory and energy loss ( $dE/dx$ ) information for charged tracks over 85% of the total solid angle. The momentum resolution is  $\sigma_p/p = 0.017\sqrt{1+p^2}$  ( $p$  in  $\text{GeV}/c$ ), and the  $dE/dx$  resolution for hadron tracks is  $\sim 8\%$ . An array of 48 scintillation counters surrounding the MDC measures the time-of-flight (TOF) of charged tracks with a resolution of  $\sim 200$  ps for hadrons. Radially outside the TOF system is a 12 radiation length, lead-gas barrel shower counter (BSC). This measures the energies of electrons and photons over  $\sim 80\%$  of the total solid angle with an energy resolution of  $\sigma_E/E = 22\%/\sqrt{E}$  ( $E$  in  $\text{GeV}$ ). Outside of the solenoid coil, which provides a 0.4 Tesla magnetic field over the tracking volume, is an iron flux return that is instrumented with three double layers of counters that identify muons with momentum greater than  $0.5 \text{ GeV}/c$ .

In order to detect the invisible  $\eta$  and  $\eta'$  decays, we use the specific  $J/\psi \rightarrow \phi\eta$  and  $\phi\eta'$  decay modes. The two-body decays of  $J/\psi$  provide us a very simple event topology as shown in Fig. 1, in which the  $\phi$  signals can be reconstructed easily and cleanly in  $K^+K^-$  final states. The reconstructed  $\phi$  can be used to tag the missing side,

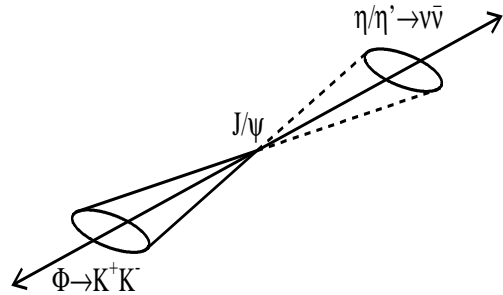


FIG. 1: Demonstration of  $J/\psi \rightarrow \phi\eta$  or  $\phi\eta'$ . The  $\phi$ , which is reconstructed in the  $K^+K^-$  final states, can be used to tag the invisible decays of the missing particles.

namely, the invisible decays of  $\eta$  and  $\eta'$ . Since both widths of  $\phi$  and  $\eta(\eta')$  are narrow and negligible by comparing with the detector resolution, the shape of the momenta of  $\phi$  is a Gaussian-like distribution. The mean values of the momentum of  $\phi$  are  $1.320 \text{ GeV}/c$  for  $J/\psi \rightarrow \phi\eta$  and  $1.192 \text{ GeV}/c$  for  $J/\psi \rightarrow \phi\eta'$ . The missing momentum  $P_{miss}$  or the missing mass  $m_{miss}$  of  $\phi$  is a powerful discriminating variable to separate signal events from possible backgrounds, in which the missed side is not from  $\eta(\eta')$  decays. The signal regions of  $\eta$  and  $\eta'$  are defined as  $|P_{miss} - 1.320| < 3\sigma_{reso}^\eta$  for  $J/\psi \rightarrow \phi\eta$  and  $|P_{miss} - 1.192| < 3\sigma_{reso}^{\eta'}$  for  $J/\psi \rightarrow \phi\eta'$ , where  $\sigma_{reso}^\eta$  (22 MeV) and  $\sigma_{reso}^{\eta'}$  (20 MeV) are detector resolutions of  $P_{miss}$  for  $J/\psi \rightarrow \phi\eta$  and  $J/\psi \rightarrow \phi\eta'$ , respectively. In addition, the strong boost of  $\phi$  is useful to define the geometrical region of the invisible decays of  $\eta$  and  $\eta'$ .

In the event selection, the total number of charged tracks is required to be two with net charge zero. Each track should have good helix fit and the polar angle  $\theta$  in MDC must satisfy  $|\cos\theta| < 0.8$ . The event must originate near the collision point; tracks must satisfy  $\sqrt{x^2 + y^2} \leq 2 \text{ cm}$ ,  $|z| \leq 20 \text{ cm}$ , where  $x$ ,  $y$  and  $z$  are space coordinates of the point of the closest approach of tracks to the beam axis. Particle identification (PID) is performed using combined TOF and  $dE/dx$  information, both charged tracks must be identified as kaon.

We consider events with no charged tracks besides those of the  $\phi \rightarrow K^+K^-$  candidate. Removing decay products of the  $\phi$  candidate from consideration, we count the number of BSC clusters consistent with a  $K_L^0$  or a

photon hypothesis,  $N_{BSC}$ . Due to accelerator-induced background and detector noise, the optimal requirements on  $N_{BSC}$  are tight. We require that  $N_{BSC}$  must be zero in the region with  $\theta_{\gamma K} > 30^\circ$ , where  $\theta_{\gamma K}$  is the open angle between charged kaon and reconstructed neutral cluster. This requirement rejects most of the backgrounds from  $\eta$  and  $\eta'$  decays into visible final states. It also reduce most of backgrounds from the multi-body decays of  $J/\psi \rightarrow \phi + \text{anything}$ . In order to ensure the final particles from  $\eta$  and  $\eta'$  decays are inside the fiducial volume of the detector, the recoiled direction of  $\phi$  is limited within the region of  $|\cos \theta_{recoil}| < 0.7$ , where  $\theta_{recoil}$  is the polar angle of the  $P_{miss}$ . Figure 2(a) shows distribution of the invariant mass of  $K^+K^-$ ,  $m_{KK}$ , after above selections in the data, a clear  $\phi$  peak is seen. Figure 2(b) shows  $P_{miss}$  distribution for the events with  $1.005 < m_{KK} < 1.035$   $\text{GeV}/c^2$ .

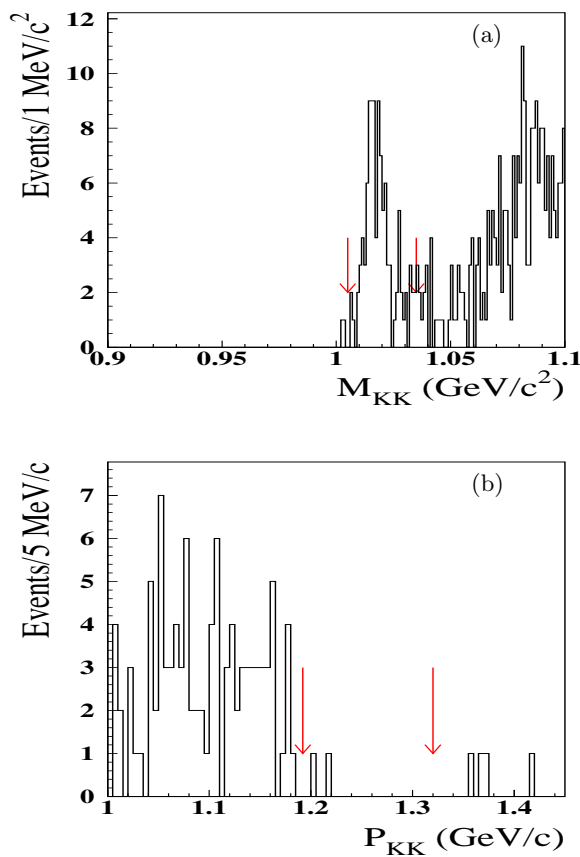


FIG. 2: (a)  $m_{KK}$  distribution after the selections from data. The arrows on the plot indicate the signal region of  $\phi$  candidates. (b)  $P_{miss}$  distribution for the events with  $1.005 < m_{KK} < 1.035$   $\text{GeV}/c^2$  in (a). The means of the missing momentum for  $J/\psi \rightarrow \phi\eta$  and  $J/\psi \rightarrow \phi\eta'$  are located around 1.32 and 1.20  $\text{GeV}/c$ , respectively, as indicated by the two arrows.

We use Monte Carlo (MC) simulated events to study the selection efficiencies for signals and possible back-

ground dilution. For signal modes, after considering the angular distribution in MC-simulated events for  $J/\psi \rightarrow \phi\eta(\eta')$  decay, we obtain about 23.5% (23.2%) selection efficiency for  $\eta$  ( $\eta'$ ). More than 20 exclusive decay modes are studied within full MC simulations in order to understand the background shapes and the expected dilution to the signal region. The sources of backgrounds are divided into two classes. Class I: the background is from  $J/\psi \rightarrow \phi\eta(\eta')$ , where  $\phi \rightarrow K^+K^-$  and  $\eta(\eta')$  decays into others except for the invisible final states. We find the expected number of background events from this class is zero for both  $\eta$  and  $\eta'$  cases. Class II: it is mainly from  $J/\psi$  decays without  $\eta$  or  $\eta'$ , such as  $\phi K_L K_L$ ,  $\phi f_0(980)(f_0(980) \rightarrow K_L K_L)$ ,  $K^{*0} K_L (K^{*0} \rightarrow K^\pm \pi^\mp)$ . The expected number of background events from class II is about  $3.0 \pm 0.2$  and  $90 \pm 64$  in the signal regions for  $\eta$  and  $\eta'$  modes, respectively.

An unbinned extended maximum likelihood (ML) fit is used to extract the event yield for  $J/\psi \rightarrow \phi\eta(\eta')$  [ $\phi \rightarrow K^+K^-$  and  $\eta(\eta') \rightarrow \text{invisible}$ ]. In the ML fit, we require that  $1.00 < P_{miss} < 1.45$   $\text{GeV}/c$ , in which the background shape is well under control as shown in Fig. 2(b). We construct probability density functions (PDFs) for the  $P_{miss}$  distributions for signals ( $\mathcal{F}_{sig}^\eta$  and  $\mathcal{F}_{sig}^{\eta'}$ ) and background ( $\mathcal{F}_{bkgd}$ ) using detailed simulations of signal and background data. The PDFs for signals are parameterized by double Gaussian distribution with common mean, one relative fraction and two distinct widths, which are all fixed to MC simulation. The PDF for background is a bifurcated Gaussian plus the first order of Polynomial ( $P_1$ ). All parameters related to background shape are floated in the nominal fit to data. The two PDFs are combined into likelihood function  $\mathcal{L}$ , defined as a function of the free parameters  $N_{sig}^\eta$ ,  $N_{sig}^{\eta'}$  and  $N_{bkgd}$

$$\mathcal{L}(N_{sig}^\eta, N_{sig}^{\eta'}, N_{bkgd}) = \frac{e^{-(N_{sig}^\eta + N_{sig}^{\eta'} + N_{bkgd})}}{N!} \times \prod_{i=1}^N [N_{sig}^\eta \mathcal{F}_{sig}^\eta(P_{miss}^i) + N_{sig}^{\eta'} \mathcal{F}_{sig}^{\eta'}(P_{miss}^i) + N_{bkgd} \mathcal{F}_{bkgd}(P_{miss}^i)], \quad (1)$$

where  $N_{sig}^\eta$  and  $N_{sig}^{\eta'}$  are the number of  $J/\psi \rightarrow \phi(\rightarrow K^+K^-)\eta(\rightarrow \text{invisible})$  and  $J/\psi \rightarrow \phi(\rightarrow K^+K^-)\eta'(\rightarrow \text{invisible})$  signal events;  $N_{bkgd}$  is the number of common background events. The fixed parameters  $N$  is the total number of selected events, and  $P_{miss}^i$  is the value of  $P_{miss}$  for the  $i$ th event. The negative log-likelihood ( $-\ln \mathcal{L}$ ) is then minimized with respect to  $N_{sig}^\eta$ ,  $N_{sig}^{\eta'}$  and  $N_{bkgd}$  in the data sample. A total 105 events enter the fit, and the resulting fitted values of  $N_{sig}^\eta$ ,  $N_{sig}^{\eta'}$  and  $N_{bkgd}$  are  $-2.84 \pm 1.44$ ,  $2.24 \pm 3.38$  and  $105.6 \pm 1.1$ , where the errors are statistical. Figure 3 shows the  $P_{miss}$  distribution and fitted results. No signal yield is observed for the invisible decay of either  $\eta$  or  $\eta'$ . We obtain upper limits

by integrating the normalized likelihood distribution over the positive values of the number of signal events. The upper limits at 90% confidence level are 3.56 events for  $\eta$  case and 5.72 events for  $\eta'$  case, respectively.

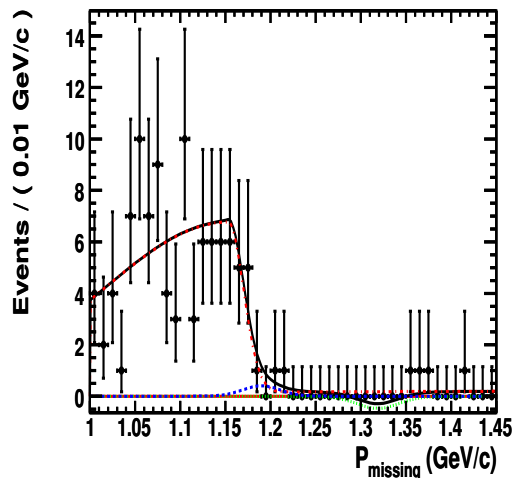


FIG. 3: The  $P_{miss}$  distribution for data sample. The data (black cross) are compared to the total fit results. The dotted curve is the projection of  $\eta$  signal component, and the dashed curve is the the projection of  $\eta'$  signal component. The dash-dotted curve is the sum of backgrounds, and the solid blue curve is the total likelihood fit results.

The branching fraction of  $\eta(\eta') \rightarrow \gamma\gamma$  is also extracted in  $J/\psi \rightarrow \phi\eta(\eta')$  decays, in order to obtain the ratio of  $\mathcal{B}(\eta(\eta') \rightarrow \text{invisible})$  and  $\mathcal{B}(\eta(\eta') \rightarrow \gamma\gamma)$ . The advantage of measuring  $\frac{\mathcal{B}(\eta(\eta') \rightarrow \text{invisible})}{\mathcal{B}(\eta(\eta') \rightarrow \gamma\gamma)}$  is that the uncertainties due to the total number of  $J/\psi$ , the tracking efficiency, PID, the number of the charged tracks, the cut on  $m_{KK}$  and residual noise of the shower counter can be canceled.

The selection criteria for the charged tracks are the same as those in the selection of  $J/\psi \rightarrow \phi\eta(\eta')$ ,  $\eta(\eta') \rightarrow \text{invisible}$  decay. While, for neutral candidates, at least two good photons are required. The candidate photon must have hits in the BSC, the number of layers hit must be greater than one, and its deposited energy in BSC is more than 50 MeV. The angle between the photon emission direction and the shower development direction of the neutral track in BSC is required to be less than  $25^\circ$ . The open angle between the candidate photon and the charged track is greater than  $30^\circ$ . The final states  $KK\gamma\gamma$  in the event are kinematically fitted using energy and momentum conservation constraints (4-C) under the hypothesis of  $J/\psi \rightarrow KK\gamma\gamma$  in order to obtain better mass resolution and suppress backgrounds further. We require the kinematic fit  $\chi^2_{K+K-\gamma\gamma}$  less than 50(15) for  $\eta(\eta')$  case. In case more than two photons in the final states, the fit is repeated using all permutations and the

combination with the best fit to  $K^+K^-\gamma\gamma$  is retained. The number of observed events for the  $J/\psi \rightarrow \phi\eta(\eta')$ ,  $\phi \rightarrow K^+K^-$  and  $\eta(\eta') \rightarrow \gamma\gamma$  decay, is obtained from the fit to the  $\gamma\gamma$  invariant mass. In Fig. 4, we show the fitted results of  $\eta(\eta') \rightarrow \gamma\gamma$ .

The contributions to the systematic error on the calculation of the ratios are summarized in Table I. Systematic errors in the ML fit originate from uncertainties in the PDF parameterizations, which arise from the limited number of events in the data sample and signal control sample. The uncertainty due to the background shape has been estimated by varying the PDF shape of the background in the ML fit.

The uncertainty, due to the requirement of no neutral cluster in BSC allowed outside the  $30^\circ$  of charged tracks, are obtained from the control sample of fully reconstructed  $J/\psi \rightarrow \phi\eta$ , where  $\eta \rightarrow \gamma\gamma$ . The efficiencies with and without the requirement of the number of extra photons are obtained. The difference of the efficiencies between data and MC, 5%, is considered as the systematic error for both  $\eta$  and  $\eta'$  cases. In fact, the purpose of this study is to check the difference of the noise in BSC (extra photons or fake photons) in the MC simulation and data sample. Compared with  $\eta \rightarrow \text{invisible}$  decay, more noise is introduced by the photons in the decay of  $\eta \rightarrow \gamma\gamma$ , so it is a conservative estimation of the systematic error for the invisible decays of  $\eta$  and  $\eta'$ .

The uncertainty in the determination of the number of the observed the  $J/\psi \rightarrow \phi\eta(\eta')$ ,  $\phi \rightarrow K^+K^-$ ,  $\eta(\eta') \rightarrow \gamma\gamma$  events is also studied. The different backgrounds shapes are tried in the fit to the  $\gamma\gamma$  invariant mass, and the variation of the fitted yields by using the different backgrounds is regarded as the systematic error, which is 2.0% (1.0%) for  $\eta(\eta')$  case. The uncertainty of photon efficiency for two photons is about 4.0% [9]. The uncertainty due to the  $\chi^2_{K+K-\gamma\gamma}$  constraints is estimated to be 1.0%(5.2%) [10] for  $\eta(\eta')$  case. The uncertainty due to trigger efficiency is also considered. The total systematic error,  $\sigma_{\eta}^{sys}$  ( $\sigma_{\eta'}^{sys}$ ),

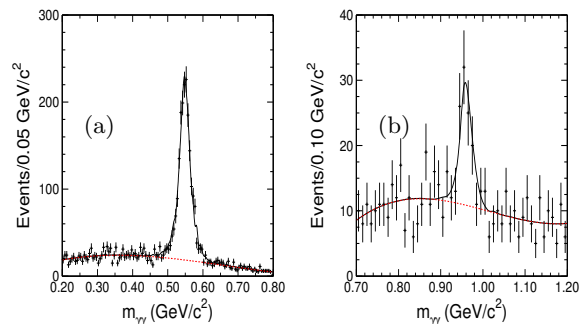


FIG. 4: (a) The fit of the  $\gamma\gamma$  invariant mass in  $J/\psi \rightarrow \phi\eta$ ,  $\eta \rightarrow \gamma\gamma$ . The dash line shows the background's component, and the solid line is the total fit result. (b) The same plot but for  $J/\psi \rightarrow \phi\eta'$ ,  $\eta' \rightarrow \gamma\gamma$ .

on the ratio is 7.65% (11.11%) for  $\eta(\eta')$  as summarized in Table I.

TABLE I: Summary of relative systematic errors on the ratios. The first three lines are from the determination of the yield of  $J/\psi \rightarrow \phi\eta(\eta')$ ,  $\eta(\eta') \rightarrow \text{invisible}$ . The next three lines are from the determination of the signal yield of the  $J/\psi \rightarrow \phi\eta(\eta')$ ,  $\eta(\eta') \rightarrow \gamma\gamma$ .

Source of Uncertainties	sys. error(%)	
	$\eta$	$\eta'$
PDF shapes in the ML fit	3.4	7.3
MC statistics	1.0	1.0
Requirement on $n_\gamma$	5.0	5.0
Photon efficiency	4.0	4.0
4-C fit for $\eta(\eta') \rightarrow \gamma\gamma$	1.0	5.2
Background shape for $\eta(\eta') \rightarrow \gamma\gamma$	2.0	1.0
Total	7.65	11.11

The upper limit on the ratio of the  $\mathcal{B}(\eta \rightarrow \text{invisible})$  and  $\mathcal{B}(\eta \rightarrow \gamma\gamma)$  is calculated with

$$\frac{\mathcal{B}(\eta \rightarrow \text{invisible})}{\mathcal{B}(\eta \rightarrow \gamma\gamma)} < \frac{n_{UL}^\eta/\epsilon_\eta}{n_{\gamma\gamma}^\eta} \cdot \frac{1}{(1 - \sigma_\eta)} \quad (2)$$

where  $n_{UL}^\eta$  is the 90% upper limit of the observed number of events for  $J/\psi \rightarrow \phi\eta$ ,  $\phi \rightarrow K^+K^-$ ,  $\eta \rightarrow \text{invisible}$  decay,  $\epsilon_\eta$  is the MC determined efficiency for the signal channel,  $n_{\gamma\gamma}^\eta$  is the number of events for the  $J/\psi \rightarrow \phi\eta$ ,  $\phi \rightarrow K^+K^-$ ,  $\eta \rightarrow \gamma\gamma$  decay after efficiency correction, and  $\sigma_\eta$  is  $\sqrt{(\sigma_\eta^{sys})^2 + (\sigma_\eta^{stat})^2} = 8.1\%$ , where  $\sigma_\eta^{sys}$  and  $\sigma_\eta^{stat}$  are the total relative systematic error for  $\eta$  case from Table I and the relative statistic error of  $n_{\gamma\gamma}^\eta$ , respectively.

While, for  $\eta'$  case,  $\sigma_{\eta'}$  is  $\sqrt{(\sigma_{\eta'}^{sys})^2 + (\sigma_{\eta'}^{stat})^2} = 21.6\%$ . The relative statistic error of the fitted yield for  $J/\psi \rightarrow \phi\eta(\eta')$ ,  $\eta(\eta') \rightarrow \gamma\gamma$ , is about 2.8%(18.5%) according to the results from the fit to the invariant mass of  $\gamma\gamma$  in Fig. 4. We also obtain the upper limit on the ratio of the  $\mathcal{B}(\eta' \rightarrow \text{invisible})$  and  $\mathcal{B}(\eta' \rightarrow \gamma\gamma)$  by replacing  $\eta$  with  $\eta'$  in Eq. (2).

TABLE II: The numbers used in the calculations of the ratios in Eq. (2), where  $n_{UL}^\eta(n_{UL}^{\eta'})$  is the upper limit of the signal events at 90% confidence level,  $\epsilon_\eta(\epsilon_{\eta'})$  is the selection efficiency,  $n_{\gamma\gamma}^\eta(n_{\gamma\gamma}^{\eta'})$  is the number of the events of  $J/\psi \rightarrow \phi\eta(\eta')$ ,  $\phi \rightarrow K^+K^-$ ,  $\eta(\eta') \rightarrow \gamma\gamma$ ,  $\sigma_\eta^{stat}(\sigma_{\eta'}^{stat})$  is the relative statistic error of  $n_{\gamma\gamma}^\eta(n_{\gamma\gamma}^{\eta'})$  and  $\sigma_\eta(\sigma_{\eta'})$  is the total relative error.

quantity	value	
	$\eta$	$\eta'$
$n_{UL}^\eta(n_{UL}^{\eta'})$	3.56	5.72
$\epsilon_\eta(\epsilon_{\eta'})$	23.5%	23.2%
$n_{\gamma\gamma}^\eta(n_{\gamma\gamma}^{\eta'})$	10,001 ± 280	471 ± 87
$\sigma_\eta^{stat}(\sigma_{\eta'}^{stat})$	2.8%	18.5%
$\sigma_\eta(\sigma_{\eta'})$	8.1%	21.6%

Using the numbers in Table II, the upper limit on the ratio of  $\mathcal{B}(\eta(\eta') \rightarrow \text{invisible})$  and  $\mathcal{B}(\eta(\eta') \rightarrow \gamma\gamma)$  is obtained at 90% confidence level of  $1.65 \times 10^{-3}$  ( $6.69 \times 10^{-2}$ ).

In summary, the invisible decay modes of  $\eta$  and  $\eta'$  are searched for the first time in the process of  $J/\psi \rightarrow \phi\eta(\eta')$  using the 58 millions  $J/\psi$  data sample at BES II. We find no signal yields for the invisible decays of  $\eta$  and  $\eta'$ , and obtain limits on the ratio,  $\frac{\mathcal{B}(\eta(\eta') \rightarrow \text{invisible})}{\mathcal{B}(\eta(\eta') \rightarrow \gamma\gamma)}$ . The upper limits at 90% confidence level are  $1.65 \times 10^{-3}$  and  $6.69 \times 10^{-2}$  for  $\frac{\mathcal{B}(\eta \rightarrow \text{invisible})}{\mathcal{B}(\eta \rightarrow \gamma\gamma)}$  and  $\frac{\mathcal{B}(\eta' \rightarrow \text{invisible})}{\mathcal{B}(\eta' \rightarrow \gamma\gamma)}$ , respectively. The advantage of measuring the ratios instead of the branching fractions of the invisible decays is that many uncertainties are canceled.

The BES collaboration thanks the staff of BEPC and computing center for their hard efforts. This work is supported in part by the National Natural Science Foundation of China under contracts Nos. 10491300, 10225524, 10225525, 10425523, the Chinese Academy of Sciences under contract No. KJ 95T-03, the 100 Talents Program of CAS under Contract Nos. U-11, U-24, U-25, and the Knowledge Innovation Project of CAS under Contract Nos. U-602, U-612, U-34 (IHEP), the National Natural Science Foundation of China under Contract No. 10225522 (Tsinghua University), and the Department of Energy under Contract No. DE-FG02-04ER41291 (U Hawaii).

- 
- [1] L. N. Chang, O. Lebedev, and J. N. Ng, Phys. Lett. **B441**, 419 (1998), hep-ph/9806487.
  - [2] B. McElrath, Phys. Rev. **D72**, 103508 (2005), hep-ph/0506151.
  - [3] G. Bertone, D. Hooper, and J. Silk, Phys. Rept. **405**, 279 (2005), hep-ph/0404175.
  - [4] P. Jean et al., Astron. Astrophys. **407**, L55 (2003), astro-ph/0309484.
  - [5] C. Boehm, D. Hooper, J. Silk, M. Casse, and J. Paul, Phys. Rev. Lett. **92**, 101301 (2004), astro-ph/0309686.
  - [6] R. Balest et al. (CLEO), Phys. Rev. **D51**, 2053 (1995).
  - [7] S. Eidelman et al. (Particle Data Group), Phys. Lett. **B592**, 1 (2004).
  - [8] J. Z. Bai et al. (BES), Nucl. Instrum. Meth. **A344**, 319 (1994).
  - [9] M. Ablikim et al. (BES), Phys. Rev. **D71**, 032003 (2005), hep-ex/0410044.
  - [10] J. Z. Bai et al. (BES), Phys. Rev. **D70**, 012005 (2004), hep-ex/0402013.